Communication: A reduced-space algorithm for the solution of the complex linear response equations used in coupled cluster damped response theory

Joanna Kauczor, Patrick Norman, Ove Christiansen and Sonia Coriani

Original Publication:

Joanna Kauczor, Patrick Norman, Ove Christiansen and Sonia Coriani, Communication: A reduced-space algorithm for the solution of the complex linear response equations used in coupled cluster damped response theory, 2013, Journal of Chemical Physics, (139), 21, 211102.
http://dx.doi.org/10.1063/1.4840275

Communication: A reduced-space algorithm for the solution of the complex linear response equations used in coupled cluster damped response theory

Joanna Kauczor, Patrick Norman, Ove Christiansen, and Sonia Coriani

Citation: The Journal of Chemical Physics **139**, 211102 (2013); doi: 10.1063/1.4840275
View online: http://dx.doi.org/10.1063/1.4840275
View Table of Contents: http://scitation.aip.org/content/aip/journal/jcp/139/21?ver=pdfcov
Published by the AIP Publishing

Communication: A reduced-space algorithm for the solution of the complex linear response equations used in coupled cluster damped response theory

Joanna Kauczor,[1] Patrick Norman,[1] Ove Christiansen,[2] and Sonia Coriani[3,a)]
[1]*Department of Physics, Chemistry and Biology, Linköping University, SE-581 83 Linköping, Sweden*
[2]*Department of Chemistry, Aarhus University, DK-8000 Aarhus C, Denmark*
[3]*Dipartimento di Scienze Chimiche e Farmaceutiche, Università degli Studi di Trieste, via L. Giorgieri 1, I-34127 Trieste, Italy*

(Received 14 October 2013; accepted 21 November 2013; published online 6 December 2013)

We present a reduced-space algorithm for solving the complex (damped) linear response equations required to compute the complex linear response function for the hierarchy of methods: coupled cluster singles, coupled cluster singles and iterative approximate doubles, and coupled cluster singles and doubles. The solver is the keystone element for the development of damped coupled cluster response methods for linear and nonlinear effects in resonant frequency regions. © *2013 AIP Publishing LLC*. [http://dx.doi.org/10.1063/1.4840275]

I. INTRODUCTION

Response theory[1,2] is a perfect framework to investigate a wealth of phenomena originating from the interaction of the electromagnetic radiation field with matter. It provides efficient computational formulas for both linear and nonlinear response properties, thus describing a plethora of optical effects.

Transition energies and (multiphoton) transition properties, as well as excited state properties, can be determined from a pole and residue analysis of response functions.[1] The generalized eigenvalue problem, usually solved for this purpose, most often relies on iterative algorithms that address only the lowest excitations. This makes the computational exploration of some of the interesting regions of the spectrum, *e.g.*, the X-ray absorption region, highly cumbersome. Alternatively, resonance spectroscopies can be accounted for by inclusion of finite excited-state lifetimes in the response functions,[3–7] hereby replacing the solution of the eigenvalue problem with the solution of "damped" linear response equations. In the complex polarization propagator (CPP) approach,[3,4] the entire frequency range may be addressed. The CPP method, implemented for Hartree–Fock and time-dependent density functional theory, has been successfully applied to simulate a variety of spectroscopies,[2,5] including UV-vis absorption, electronic circular dichroism, magnetic circular dichroism, two-photon absorption, near-edge X-ray absorption cross-section, and X-ray circular dichroism. An important step in this development has been the implementation of an efficient solver[8] for the damped response equations that has increased the range of applicability of the methodology to nanoparticles.[9–11]

Coupled cluster (CC) response methods[12,13] are considered among the most accurate tools for determining spectroscopic properties. However, rather limited attempts have so far been made to extend their applicability in the high-energy region. We have recently taken this path, and implemented a Lanczos-based approach[14,15] that has the advantage of yielding a global pseudo-spectrum that includes the X-ray region, and that can also be coupled to Stieltjes imaging to obtain total photoionization cross-section profiles.[16] However, it suffers by intrinsic limitations, in particular a lack of *a priori* control of the convergence, due to the fact that the size of the truncated excitation space (the so-called "chain length") needs to be specified as input information. To verify convergence, calculations at various chain lengths are typically required. For X-ray spectroscopies, rather large chain lengths are required to obtain a sufficient description of the X-ray spectrum, which highly increases the computational cost of this procedure.[14,15,17]

The definition and implementation of an iterative subspace algorithm for solving the damped CC response equations presented in this communication is thus an important achievement and can be considered a key element in the extension of the CPP formalism to higher order damped CC response functions.

II. THE COMPLEX COUPLED CLUSTER LINEAR RESPONSE FUNCTION

In exact theory, the linear response function $\langle\langle X; Y\rangle\rangle_\omega$ for two generic operators X and Y is given by

$$\langle\langle X; Y\rangle\rangle_\omega = -\sum_j \left[\frac{\langle 0|X|j\rangle\langle j|Y|0\rangle}{\omega_j - \omega} + \frac{\langle 0|Y|j\rangle\langle j|X|0\rangle}{\omega_j + \omega} \right], \tag{1}$$

and it diverges when the frequency ω of the external field approaches any of the transition frequencies ω_j of the system. Damping terms, the finite lifetime parameters that correspond to line-broadenings in absorption spectra, can be introduced in the linear response function,[3,4] thereby yielding the *damped* linear response function. By adopting a common damping

a)Author to whom correspondence should be addressed. Electronic mail: coriani@units.it

parameter γ for all excited states, one can write

$$\langle\langle X;Y\rangle\rangle_{\omega}^{\gamma} = -\sum_{j}\left[\frac{\langle 0|X|j\rangle\langle j|Y|0\rangle}{\omega_j - (\omega + i\gamma)} + \frac{\langle 0|Y|j\rangle\langle j|X|0\rangle}{\omega_j + (\omega + i\gamma)}\right], \tag{2}$$

where the imaginary term $i\gamma$ is associated with the external frequency ω, rather than the transition frequency ω_j. Thus, damped linear response theory effectively corresponds to introducing a complex optical frequency $\omega \to \omega + i\gamma$, which implies solving linear response equations with complex frequencies.[3,4,7]

In analogy with the exact case, the damped equivalent of the well-known CC linear response function is obtained by replacing the frequency ω by the complex frequency $\omega + i\gamma$,

$$\begin{aligned}\langle\langle X;Y\rangle\rangle_{\omega}^{\gamma} = C^{\pm(\omega)}\big\{&\eta_{\mu}^{X}t_{\mu}^{Y}(\omega + i\gamma) + \eta_{\mu}^{Y}t_{\mu}^{X}(-\omega - i\gamma)\\ &+F_{\mu\nu}t_{\mu}^{X}(-\omega - i\gamma)t_{\nu}^{Y}(\omega + i\gamma)\big\},\end{aligned} \tag{3}$$

where $C^{\pm\omega}$ is a symmetrization operator, $C^{\pm\omega}f(\omega) = \{f(\omega) + f^{*}(-\omega)\}$. Summation over repeated indices is implied here and throughout. Calculating Eq. (3) requires the solution of the complex CC linear response equations of the form

$$[\boldsymbol{A} - (\omega + i\gamma)\mathbf{1}]\boldsymbol{t}^{Y}(\omega + i\gamma) = -\boldsymbol{\xi}^{Y}, \tag{4}$$

where $\boldsymbol{A}$ is the real asymmetric CC Jacobian matrix[12]

$$A_{\mu\nu} = \langle\mu|\exp(-T)[H,\tau_{\nu}]\exp(T)|\mathrm{HF}\rangle, \tag{5}$$

and the right-hand-side vector $\boldsymbol{\xi}^{Y}$ has the form[12]

$$\xi_{\mu}^{Y} = \langle\mu|\exp(-T)Y\exp(T)|\mathrm{HF}\rangle. \tag{6}$$

We furthermore need

$$\eta_{\nu}^{X} = \langle\Lambda|[X,\tau_{\nu}]|\mathrm{CC}\rangle, \tag{7}$$

$$F_{\mu\nu} = \langle\Lambda|[[H,\tau_{\mu}],\tau_{\nu}]|\mathrm{CC}\rangle, \tag{8}$$

where $|\mathrm{CC}\rangle = \exp(T)|\mathrm{HF}\rangle$, T is the cluster operator, $T = \sum_{\mu}t_{\mu}\tau_{\mu}$, with t_{μ} indicating the cluster amplitude and τ_{μ} the excitation operator of excitation μ. In addition, the so-called Lambda state[12] $\langle\Lambda| = \langle\mathrm{HF}| + \sum_{\lambda}\bar{t}_{\lambda}\langle\lambda|\exp(-T)$ has been introduced. The Hartree–Fock reference state, $|\mathrm{HF}\rangle$, as well as the t_{μ} and $\bar{t}_{\lambda}$ parameters are assumed to be real. In the $\gamma \to 0$ limit, Eq. (3) becomes the standard CC response function (in its symmetrized form).[12] As an additional proof of this form, it was shown in Ref.18 that Eq. (3) gives the exact damped response function in the limit of a complete cluster expansion.

In our previous work,[14,15] we have illustrated how the damped response function can be computed in a diagonal Lanczos basis of pseudo-eigenvectors. In the following, we instead illustrate an efficient way to directly solve the CC complex linear response equations of the CPP approach and thereby obtain the damped linear response functions similar to what is conventionally done in non-resonant response theory.

III. THE COMPLEX COUPLED CLUSTER LINEAR RESPONSE SOLVER

Absorption and dispersion spectra may be obtained from the solution to a complex linear equation of the form

$$(\boldsymbol{A} - (\omega + i\gamma)\mathbf{1})(\boldsymbol{t}^{R} + i\boldsymbol{t}^{I}) = -(\boldsymbol{\xi}^{R} + i\boldsymbol{\xi}^{I}), \tag{9}$$

where the superscript Y in Eq. (4) has been omitted, and real (R) and imaginary (I) components of the solution vector $\boldsymbol{t}^{Y}$ and right-hand-side vector $\boldsymbol{\xi}^{Y}$ have been explicitly introduced. Note that for real operators $\boldsymbol{\xi}^{I} = \mathbf{0}$. Equation (9) may be written in a "pseudo-symmetric" real matrix form

$$\begin{pmatrix}(\boldsymbol{A} - \omega\mathbf{1}) & \gamma\mathbf{1}\\ \gamma\mathbf{1} & -(\boldsymbol{A} - \omega\mathbf{1})\end{pmatrix}\begin{pmatrix}\boldsymbol{t}^{R}\\ \boldsymbol{t}^{I}\end{pmatrix} = \begin{pmatrix}-\boldsymbol{\xi}^{R}\\ \boldsymbol{\xi}^{I}\end{pmatrix}, \tag{10}$$

where the coupling between the different components is explicitly considered. The solution to Eq. (9) may be obtained in a reduced subspace using an iterative subspace algorithm, similar in spirit to previous work for electronic structure methods with symmetric matrices in their response equations.[8]

After the nth iteration, sets of k real orthonormal trial vectors

$$\boldsymbol{b}^{k} = \{\boldsymbol{b}_1, \boldsymbol{b}_2, \boldsymbol{b}_3, \boldsymbol{b}_4, \ldots, \boldsymbol{b}_{k-1}, \boldsymbol{b}_k\}, \tag{11}$$

and the corresponding linear transformed vectors

$$\boldsymbol{\rho}^{k} = \{\boldsymbol{A}\boldsymbol{b}_1, \boldsymbol{A}\boldsymbol{b}_2, \boldsymbol{A}\boldsymbol{b}_3, \boldsymbol{A}\boldsymbol{b}_4, \ldots, \boldsymbol{A}\boldsymbol{b}_{k-1}, \boldsymbol{A}\boldsymbol{b}_k\} \tag{12}$$

are known, where $k \leq 2n$ due to orthonormalization (see later). Equation (10) is solved in the reduced space spanned by $\boldsymbol{b}^{k}$ in Eq. (11), i.e., by solving

$$\begin{pmatrix}\boldsymbol{A}_{\mathrm{red}} - \omega\mathbf{1}_{\mathrm{red}} & \gamma\mathbf{1}_{\mathrm{red}}\\ \gamma\mathbf{1}_{\mathrm{red}} & -(\boldsymbol{A}_{\mathrm{red}} - \omega\mathbf{1}_{\mathrm{red}})\end{pmatrix}\begin{pmatrix}\boldsymbol{x}^{R}\\ \boldsymbol{x}^{I}\end{pmatrix} = \begin{pmatrix}-\boldsymbol{\xi}_{\mathrm{red}}^{R}\\ \boldsymbol{\xi}_{\mathrm{red}}^{I}\end{pmatrix}, \tag{13}$$

where

$$[\boldsymbol{\xi}_{\mathrm{red}}^{R}]_i = \boldsymbol{b}_i^{T}\boldsymbol{\xi}^{R}, \quad [\boldsymbol{\xi}_{\mathrm{red}}^{I}]_i = \boldsymbol{b}_i^{T}\boldsymbol{\xi}^{I}, \tag{14}$$

$$[\boldsymbol{A}_{\mathrm{red}}]_{ij} = \boldsymbol{b}_i^{T}(\boldsymbol{\rho}^{k})_j = \boldsymbol{b}_i^{T}\boldsymbol{A}\boldsymbol{b}_j, \tag{15}$$

and $\mathbf{1}_{\mathrm{red}}$ is a unit matrix of dimension $k \times k$. Solving Eq. (13) yields the optimal solution vector with real and imaginary components given as

$$\boldsymbol{t}_{n+1}^{R} = \sum_{i=1}^{k}x_i^{R}\boldsymbol{b}_i, \quad \boldsymbol{t}_{n+1}^{I} = \sum_{i=1}^{k}x_i^{I}\boldsymbol{b}_i. \tag{16}$$

The residual ($\boldsymbol{R}$) is calculated to check for convergence and its real and imaginary components have the form

$$\begin{aligned}\boldsymbol{R}_{n+1}^{R} &= (\boldsymbol{A} - \omega\mathbf{1})\boldsymbol{t}_{n+1}^{R} + \gamma\mathbf{1}\boldsymbol{t}_{n+1}^{I} + \boldsymbol{\xi}^{R}\\ &= \sum_{i=1}^{k}x_i^{R}(\boldsymbol{\rho}^{k})_i - \omega\sum_{i=1}^{k}x_i^{R}\boldsymbol{b}_i + \gamma\sum_{i=1}^{k}x_i^{I}\boldsymbol{b}_i + \boldsymbol{\xi}^{R},\end{aligned} \tag{17}$$

$$\boldsymbol{R}^I_{n+1} = -(\boldsymbol{A}-\omega\mathbf{1})\boldsymbol{t}^I_{n+1} + \gamma\mathbf{1}\boldsymbol{t}^R_{n+1} - \boldsymbol{\xi}^I$$
$$= -\sum_{i=1}^{k} x^I_i(\boldsymbol{\rho}^k)_i + \omega\sum_{i=1}^{k} x^I_i\boldsymbol{b}_i + \gamma\sum_{i=1}^{k} x^R_i\boldsymbol{b}_i - \boldsymbol{\xi}^I, \quad (18)$$

respectively. The residuals are used to obtain additional trial vectors by means of preconditioning (as described in Ref. 8)

$$\begin{pmatrix}\boldsymbol{b}^R_{n+1}\\ \boldsymbol{b}^I_{n+1}\end{pmatrix} = [(\boldsymbol{A}_0-\omega\mathbf{1})^2+\gamma^2\mathbf{1}]^{-1} \otimes \begin{pmatrix}(\boldsymbol{A}_0-\omega\mathbf{1}) & \gamma\mathbf{1}\\ \gamma\mathbf{1} & -(\boldsymbol{A}_0-\omega\mathbf{1})\end{pmatrix}\begin{pmatrix}\boldsymbol{R}^R_{n+1}\\ \boldsymbol{R}^I_{n+1}\end{pmatrix}, \quad (19)$$

where $\boldsymbol{A}_0$ is a diagonal approximation of $\boldsymbol{A}$, which amounts to differences of orbital energies in the zeroth-order approximation. The new trial vectors $\boldsymbol{b}^R_{n+1}$ and $\boldsymbol{b}^I_{n+1}$ are then orthogonalized against all previous vectors in the set in Eq. (11), and are, if not below a given threshold, normalized and added to the subspace $\boldsymbol{b}^k$ as $\boldsymbol{b}_{k+1}$ and $\boldsymbol{b}_{k+2}$. The iteration procedure is continued until convergence is obtained, i.e., until the Euclidean norm of the residual, $||\boldsymbol{R}||$, is smaller than a preset threshold. In practice, a relative residual norm is used, relative to the norm of the property gradient ξ^Y, or, alternatively, the norm of the optimal solution vector. The preconditioned and orthonormalized right-hand side vectors are used as start vectors in the algorithm.

IV. RESULTS

The proposed CC-CPP algorithm has been implemented in a development version of DALTON.[19] We present below a pilot illustration of its performance via computations of the near-edge X-ray absorption fine structure (NEXAFS) spectrum of ethene. Calculations have been performed at the coupled cluster singles and doubles (CCSD) level of theory using the aug-cc-pCVDZ and cc-pVDZ basis sets[20,21] on carbon and hydrogen, respectively, plus a set of Rydberg functions[22] placed in the center of mass, as done in Ref. 17. The relaxation parameter that governs the broadening of the absorption spectrum has been chosen as $\gamma = 1000\ \mathrm{cm}^{-1}$ and the response equations have been solved to a threshold of 10^{-8} relative to the norm of the optimal solution vector. The results from the Lanczos-based algorithm with a large chain length of 4000 are taken from Ref. 17.

Figure 1 illustrates the NEXAFS spectrum obtained using the CC-CPP solver (upper panel) and the Lanczos-based algorithm (bottom panel). The plotted linear absorption cross-section, $\sigma(\omega)$, is given as

$$\sigma(\omega) = \frac{4\pi\omega}{c}\mathrm{Im}\left[\alpha^{\gamma}_{\beta\beta}(\omega)\right] = -\frac{4\pi\omega}{c}\mathrm{Im}\langle\langle\mu_\beta;\mu_\beta\rangle\rangle^{\gamma}_{\omega}. \quad (20)$$

The components of the dipole polarizability (including γ) are obtained from the linear response function as $\alpha^{\gamma}_{\beta\beta}(\omega) = -\langle\langle\mu_\beta;\mu_\beta\rangle\rangle^{\gamma}_{\omega}$, where μ_β indicates a Cartesian component of the electric-dipole operator. The CC-CPP results have been obtained directly in the frequency region between 286 and 292 eV. From the comparison between the two panels, it can be seen that the spectra calculated using both algorithms are in perfect agreement. In the following, we concentrate our analysis on the strongest absorption peak, describing the $1s \rightarrow \pi^*$ transition, centered at 287.47 eV and polarized in the x direction.

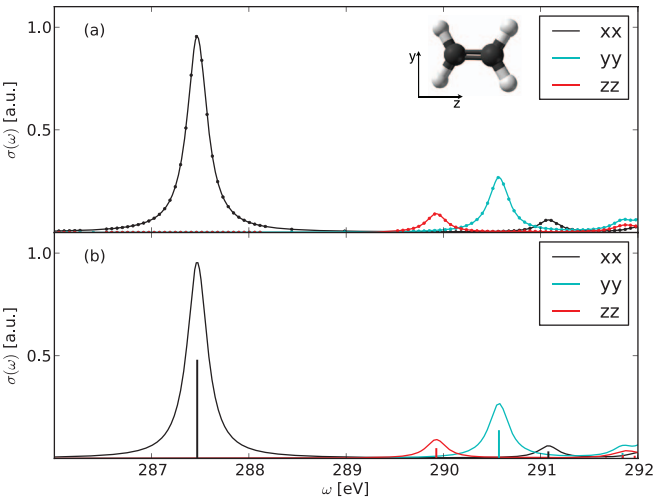

FIG. 1. NEXAFS spectrum [xx- (black), yy- (red), and zz- (blue) component] of ethene at the CCSD level obtained with the (a) CC-CPP and (b) Lanczos-based solver. Lanczos chain length is 4000, $\gamma = 1000\ \mathrm{cm}^{-1}$, and threshold is 10^{-8}.

In Table I, the real and imaginary components of the complex dipole polarizability obtained with the CC-CPP solver, for selected frequencies in the resonant region, are compared with the corresponding values computed using the Lanczos-based algorithm. The results are in an excellent agreement with each other. For the CC-CPP solver it was checked that all digits reported are converged. In the Lanczos-based algorithm the whole spectrum is addressed, but there is a chain-length dependent error for a specific frequency. With a large chain-length of 4000 there is only a very minor discrepancy between the two sets of numbers in Table I, due to the use of a finite chain length in the Lanczos simulation.

Figure 2 illustrates the convergence characteristics of the CC-CPP algorithm at four frequency values (and their negative counterparts), in the proximity of the $1s \rightarrow \pi^*$ resonance.

TABLE I. Real and imaginary components of the electric-dipole polarizability $\alpha^{\gamma}_{xx}(\omega)$ at selected frequencies. Results are obtained using the CC-CPP and the Lanczos-based (chain length of 4000) solvers at the CCSD level of theory, with $\gamma = 1000\ \mathrm{cm}^{-1}$ and a relative threshold of 10^{-8}.

Algorithm	ω (eV)	$\mathrm{Re}\left[\alpha^{\gamma}_{xx}(\omega)\right]$	$\mathrm{Im}\left[\alpha^{\gamma}_{xx}(\omega)\right]$
CC-CPP	287.24	1.2089087	0.6903956
Lanczos	287.24	1.2088669	0.6904238
CC-CPP	287.35	1.4369063	1.5770925
Lanczos	287.35	1.4367912	1.5770884
CC-CPP	287.46	0.1381132	2.9562324
Lanczos	287.46	0.1380810	2.9560186
CC-CPP	287.57	− 1.4952012	1.7802092
Lanczos	287.57	− 1.4950742	1.7801796
CC-CPP	287.68	− 1.3393618	0.7670029
Lanczos	287.68	− 1.3393117	0.7670286

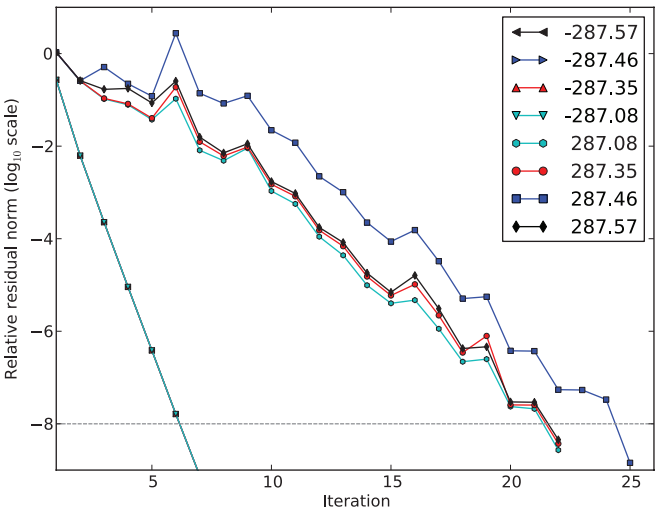

FIG. 2. Relative residual norm versus number of CC-CPP solver iterations to obtain the response amplitudes $\boldsymbol{t}^X(\omega + i\gamma)$ at chosen frequencies (given in the legend). The value of the damping parameter is $\gamma = 1000$ cm^{-1}. The relative threshold of convergence at 10^{-8} is indicated by a horizontal line. Note that the trend lines of the four negative frequencies (converging in 7 iterations) overlap completely.

The calculation has been performed for 10 positive frequencies in the resonant region: from 287.08 to 287.57 eV with a step of ≈0.05 eV (0.002 a.u.) and their negative counterparts, i.e., 20 equations have been solved simultaneously. We observe rapid convergence (in 7 iterations) for the negative frequencies due to the fact that they are far from any resonance. At resonance frequencies, convergence is expected to be the slowest (see Ref.8 for a detailed discussion), and yet only 25 iterations are required to obtain the solution vector at ω=287.46 eV. The remaining equations converged with about the same rate in 22 iterations. Convergence in an off-resonant region is much faster.

V. CONCLUDING REMARKS

We have presented an implementation of an algorithm to solve the complex response equations of damped coupled cluster response theory. Pilot results have been reported for the NEXAFS of ethene and compared with the results obtained with our previous asymmetric Lanczos-based solver. In difference to the Lanczos-based solver, the CC-CPP solver allows us to target a specific and arbitrarily narrow frequency region, with *a priori* control on the convergence of the solution vectors. The algorithm shows convergence features analogous to the solver for the linear response equations of standard (non-resonant) coupled cluster response theory, i.e., at most 25 iterations are required to reach a relative convergence threshold of 10^{-8}. The solver represents a keystone element for further development of damped CC response methods for linear and nonlinear effects in resonant frequency regions.

ACKNOWLEDGMENTS

J.K. and P.N. acknowledge financial support from the Swedish Research Council (Grant No. 621-2010-5014). O.C. acknowledges support from the Danish National Research Foundation and Danish e-infrastructure cooperation (DeiC). S.C. acknowledges support from the FP7-PEOPLE-2009-IEF funding scheme (Project No. 254326) and from the Italian MIUR (PRIN2009 Grant No. 2009C28YBF_001).

[1] J. Olsen and P. Jørgensen, J. Chem. Phys. **82**, 3235 (1985).
[2] T. Helgaker, S. Coriani, K. Kristensen, P. Jørgensen, J. Olsen, and K. Ruud, Chem. Rev. **112**, 543 (2012).
[3] P. Norman, D. M. Bishop, H. J. Aa. Jensen, and J. Oddershede, J. Chem. Phys. **115**, 10323 (2001).
[4] P. Norman, D. M. Bishop, H. J. Aa. Jensen, and J. Oddershede, J. Chem. Phys. **123**, 194103 (2005).
[5] P. Norman, Phys. Chem. Chem. Phys. **13**, 20519 (2011).
[6] L. Jensen, J. Autschbach, and G. Schatz, J. Chem. Phys. **122**, 224115 (2005).
[7] K. Kristensen, J. Kauczor, T. Kjærgaard, and P. Jørgensen, J. Chem. Phys. **131**, 044112 (2009).
[8] J. Kauczor, P. Jørgensen, and P. Norman, J. Chem. Theory Comput. **7**, 1610 (2011).
[9] M. Ahrén, L. Selegård, F. Söderlind, M. Linares, J. Kauczor, P. Norman, P.-O. Käll, and K. Uvdal, J. Nanopart. Res. **14**, 1006 (2012).
[10] J. Kauczor, P. Norman, and W. A. Saidi, J. Chem. Phys. **138**, 114107 (2013).
[11] T. Fahleson, J. Kauczor, P. Norman, and S. Coriani, Mol. Phys. **111**, 1401 (2013).
[12] O. Christiansen, C. Hättig, and P. Jørgensen, Int. J. Quantum Chem. **68**, 1 (1998).
[13] T. B. Pedersen and H. Koch, J. Chem. Phys. **108**, 5194 (1998).
[14] S. Coriani, O. Christiansen, T. Fransson, and P. Norman, Phys. Rev. A **85**, 022507 (2012).
[15] S. Coriani, T. Fransson, O. Christiansen, and P. Norman, J. Chem. Theory Comput. **8**(5), 1616 (2012).
[16] J. Cukras, S. Coriani, P. Decleva, O. Christiansen, and P. Norman, J. Chem. Phys. **139**, 094103 (2013).
[17] T. Fransson, S. Coriani, O. Christiansen, and P. Norman, J. Chem. Phys. **138**, 124311 (2013).
[18] B. Thomsen, M. Hansen, P. Seidler, and O. Christiansen, J. Chem. Phys. **136**, 124101 (2012).
[19] K. Aidas, C. Angeli, K. L. Bak, V. Bakken, R. Bast, L. Boman, O. Christiansen, R. Cimiraglia, S. Coriani, P. Dahle, E. K. Dalskov, U. Ekström, T. Enevoldsen, J. J. Eriksen, P. Ettenhuber, B. Fernández, L. Ferrighi, H. Fliegl, L. Frediani, K. Hald, A. Halkier, C. Hättig, H. Heiberg, T. Helgaker, A. C. Hennum, H. Hettema, E. Hjertenæs, S. Høst, I.-M. Høyvik, M. F. Iozzi, B. Jansik, H. J. Aa. Jensen, D. Jonsson, P. Jørgensen, J. Kauczor, S. Kirpekar, T. Kjærgaard, W. Klopper, S. Knecht, R. Kobayashi, H. Koch, J. Kongsted, A. Krapp, K. Kristensen, A. Ligabue, O. B. Lutnæs, J. I. Melo, K. V. Mikkelsen, R. H. Myhre, C. Neiss, C. B. Nielsen, P. Norman, J. Olsen, J. M. H. Olsen, A. Osted, M. J. Packer, F. Pawlowski, T. B. Pedersen, P. F. Provasi, S. Reine, Z. Rinkevicius, T. A. Ruden, K. Ruud, V. Rybkin, P. Salek, C. C. M. Samson, A. Sánchez de Merás, T. Saue, S. P. A. Sauer, B. Schimmelpfennig, K. Sneskov, A. H. Steindal, K. O. Sylvester-Hvid, P. R. Taylor, A. M. Teale, E. I. Tellgren, D. P. Tew, A. J. Thorvaldsen, L. Thøgersen, O. Vahtras, M. A. Watson, D. J. D. Wilson, M. Ziolkowski, and H. Ågren, "The Dalton quantum chemistry program system," WIREs Comput. Mol. Sci. (published online).
[20] T. H. Dunning, J. Chem. Phys. **90**, 1007 (1989).
[21] D. E. Woon and T. H. Dunning, J. Chem. Phys. **100**, 2975 (1994); **103**, 4572 (1995).
[22] K. Kaufmann, W. Baumeister, and M. Jungen, J. Phys. B: At. Mol. Opt. Phys. **22**, 2223 (1989).